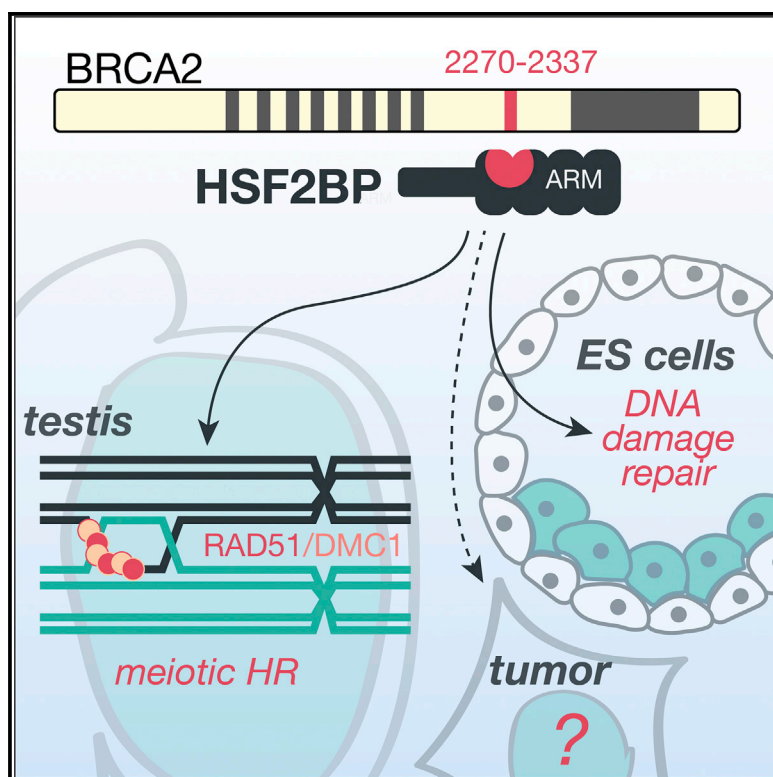


HSF2BP Interacts with a Conserved Domain of BRCA2 and Is Required for Mouse Spermatogenesis

Graphical Abstract



Authors

Inger Brandsma, Koichi Sato,
Sari E. van Rossum-Fikkert, ...,
Puck Knipscheer, Roland Kanaar,
Alex N. Zelensky

Correspondence

p.knipscheer@hubrecht.eu (P.K.),
r.kanaar@erasmusmc.nl (R.K.),
a.zelensky@erasmusmc.nl (A.N.Z.)

In Brief

BRCA2 is a key homologous recombination mediator in vertebrates. Brandsma et al. show that it directly interacts with a testis-expressed protein, HSF2BP, and that male mice deficient for HSF2BP are infertile due to a meiotic recombination defect. They also find that HSF2BP contributes to DNA repair in mouse embryonic stem cells.

Highlights

- HSF2BP forms a direct evolutionarily conserved interaction with BRCA2
- Loss of HSF2BP disrupts meiotic homologous recombination in spermatogenesis
- In addition to testis, HSF2BP also functions in mouse embryonic stem cells
- *HSF2BP* is transcribed widely in cancer cells and overexpressed in some tumors



HSF2BP Interacts with a Conserved Domain of BRCA2 and Is Required for Mouse Spermatogenesis

Inger Brandsma,^{1,8} Koichi Sato,² Sari E. van Rossum-Fikkert,^{1,3} Nicole van Vliet,¹ Esther Sleddens,⁴ Marcel Reuter,¹ Hanny Odijk,¹ Nathalie van den Tempel,¹ Dick H.W. Dekkers,⁵ Karel Bezstarosti,⁵ Jeroen A.A. Demmers,⁵ Alex Maas,⁶ Joyce Lebbink,^{1,3} Claire Wyman,^{1,3} Jeroen Essers,^{1,3,7} Dik C. van Gent,¹ Willy M. Baarends,⁴ Puck Knipscheer,^{2,*} Roland Kanaar,^{1,*} and Alex N. Zelensky^{1,9,*}

¹Department of Molecular Genetics, Oncode Institute, Erasmus University Medical Center, 3000 CA Rotterdam, the Netherlands

²Oncode Institute, Hubrecht Institute-KNAW and University Medical Center Utrecht, 3584 CT Utrecht, the Netherlands

³Department of Radiation Oncology, Erasmus University Medical Center, 3000 CA Rotterdam, the Netherlands

⁴Department of Developmental Biology, Erasmus University Medical Center, 3000 CA Rotterdam, the Netherlands

⁵Proteomics Center, Erasmus University Medical Center, 3000 CA Rotterdam, the Netherlands

⁶Department of Cell Biology, Erasmus University Medical Center, 3000 CA Rotterdam, the Netherlands

⁷Department of Vascular Surgery, Erasmus University Medical Center, 3000 CA Rotterdam, the Netherlands

⁸Present address: Toxys B.V., 2333 CG Leiden, the Netherlands

*Lead Contact

*Correspondence: p.knipscheer@hubrecht.eu (P.K.), r.kanaar@erasmusmc.nl (R.K.), a.zelensky@erasmusmc.nl (A.N.Z.)

<https://doi.org/10.1016/j.celrep.2019.05.096>

SUMMARY

The tumor suppressor BRCA2 is essential for homologous recombination (HR), replication fork stability, and DNA interstrand crosslink repair in vertebrates. We identify HSF2BP, a protein previously described as testis specific and not characterized functionally, as an interactor of BRCA2 in mouse embryonic stem cells, where the 2 proteins form a constitutive complex. HSF2BP is transcribed in all cultured human cancer cell lines tested and elevated in some tumor samples. Inactivation of the mouse *Hsf2bp* gene results in male infertility due to a severe HR defect during spermatogenesis. The BRCA2-HSF2BP interaction is highly evolutionarily conserved and maps to armadillo repeats in HSF2BP and a 68-amino acid region between the BRC repeats and the DNA binding domain of human BRCA2 (Gly2270-Thr2337) encoded by exons 12 and 13. This region of BRCA2 does not harbor known cancer-associated missense mutations and may be involved in the reproductive rather than the tumor-suppressing function of BRCA2.

INTRODUCTION

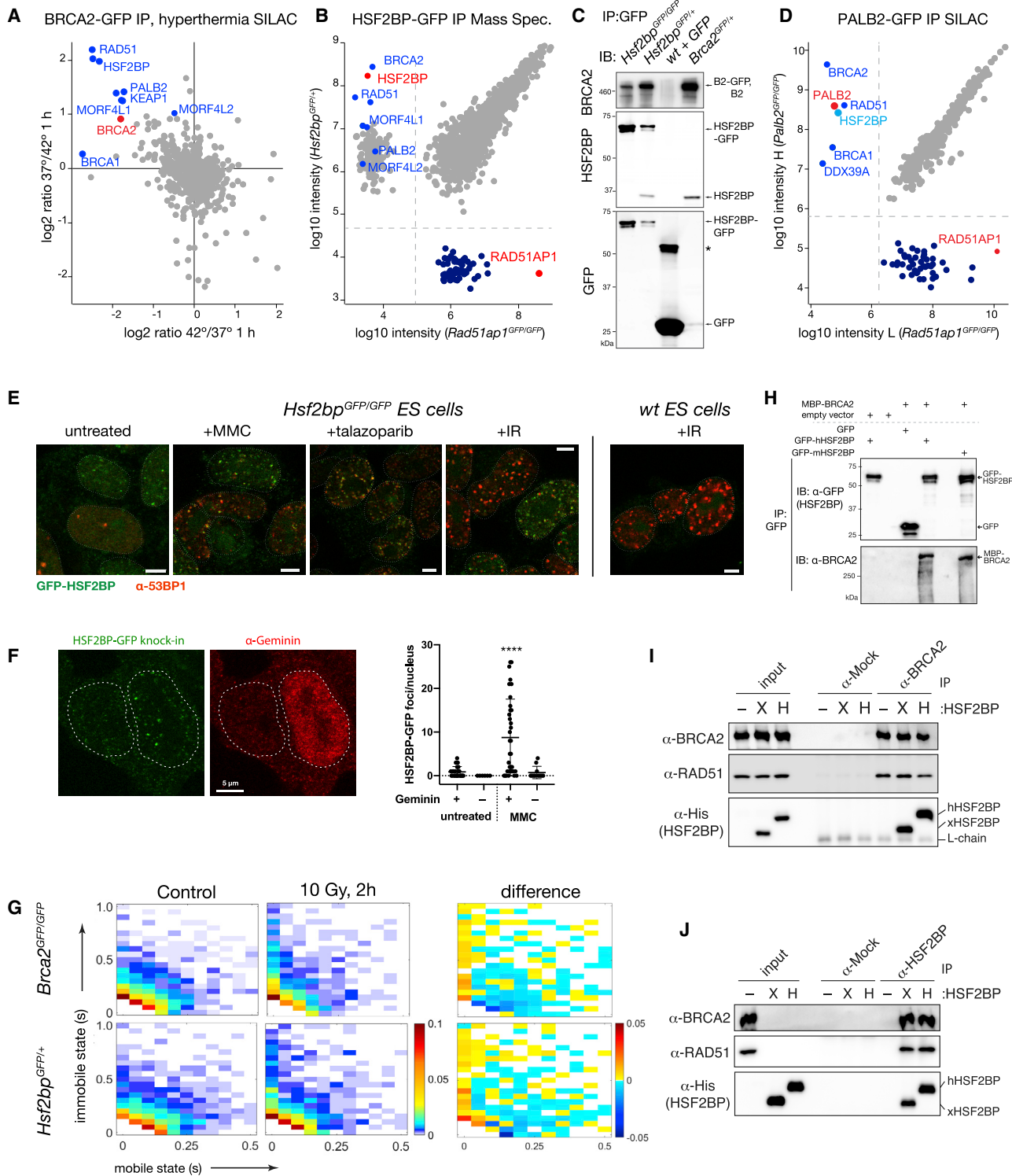
Breast cancer-associated protein 2 (BRCA2) has been the subject of intense research because of its role as a tumor suppressor and the mediator of homologous recombination (HR) in vertebrates, yet many important questions remain open (reviewed in Prakash et al., 2015; Roy et al., 2011; Zelensky et al., 2014). A major breakthrough in the understanding of the molecular function of BRCA2 came from the discovery that it interacts—primarily via a set of short BRC repeats—with the eukaryotic strand exchange protein RAD51 (Chen et al., 1998; Pellegrini

et al., 2002; Sharan et al., 1997; Wong et al., 1997). This connected BRCA2 to what is now believed to be its main role: facilitating proper RAD51 function in various HR contexts. Studying BRCA2 interactions with other proteins, known (Martinez et al., 2015) and yet undiscovered, will help address some of the unresolved questions.

BRCA2 appears to be essential for all forms of RAD51-mediated HR in both mitotic and meiotic cells. In somatic cells, HR is commonly described as an error-free pathway for the repair of DNA double-strand breaks (DSBs), but this type of damage can also be handled by various forms of non-homologous end joining. DNA replication, however, creates problematic DNA structures, such as one-ended DSBs from replication fork collapse or collisions between the fork and DNA interstrand crosslink (ICL), which can only be resolved by HR. The chemical complexity of ICLs, which compromise both DNA strands, necessitates a sophisticated set of enzymes and signaling proteins (22 identified to date, including BRCA2 and RAD51) referred to as the Fanconi anemia (FA) pathway (Inano et al., 2017; Kottemann and Smogorzewska, 2013).

In eukaryotes, HR is also required for the repair of meiotic DSBs formed by a nuclease complex containing SPO11 and TOPOVIBL (Robert et al., 2016). Formation and repair of these DSBs is required for homologous chromosome pairing and for the formation of crossovers, which, together with sister chromatid cohesion, ensure the correct separation of the homologs during the first division of meiosis (Inagaki et al., 2010; Zickler and Kleckner, 2015). Many events in meiotic HR are similar to what happens during DSB repair in somatic cells, and proteins that are essential for mitotic HR are also required in meiosis (Kuznetsov et al., 2007; Sharan et al., 2004; Simhadri et al., 2014; Xu et al., 2003). The meiotic role of BRCA2 is conserved in invertebrate, plant, and fungal homologs, despite differences in domain organization and low overall protein sequence conservation (Klovstad et al., 2008; Kojic et al., 2002; Seeliger et al., 2012; Siaud et al., 2004). FA pathway proteins also play a role in meiotic DSB repair, and mutations in FA pathway genes in both mice and



**Figure 1. Identification of HSF2BP as a BRCA2-Interacting Protein**

(A) SILAC ratios from mass spectrometric analysis of anti-GFP co-immunoprecipitates (coIPs) from *Brca2*^{GFP/GFP} mESCs (exposed to 42°C and control). Known members of the BRCA complex are indicated.

(B) Mass spectrometry of GFP coIPs from *Hsf2bp*^{GFP/+} and *Rad51ap1*^{GFP/GFP} cells. Combined peptide intensities are plotted; missing values were imputed (dotted lines; see Method Details).

(legend continued on next page)

humans lead to meiotic defects (Alavattam et al., 2016). Despite the fact that many components of HR in somatic and meiotic cells are shared, certain steps are specifically adapted in meiosis to avoid usage of the sister chromatid as the repair template and/or stimulate the incorporation of one of the chromatids of the homologous chromosomes into the HR process (interhomolog bias). This meiotic specialization of HR is achieved at least in part through the actions of specialized meiotic paralogs of DNA metabolism proteins. For example, meiocytes express DMC1, a meiosis-specific paralog of RAD51. It is essential for meiotic HR and interacts with the conserved PhePP motif and the BRC repeats of BRCA2 (Martinez et al., 2016; Thorslund et al., 2007). Why both of these strand exchange proteins are required in meiosis, how BRCA2 chaperones them to ensure their proper function, and what other domains of BRCA2 may be contributing to meiotic HR are the subjects of ongoing investigation (Abreu et al., 2018).

In this report, we describe a direct and highly evolutionarily conserved interaction of BRCA2 with HSF2BP, a protein previously only identified in testis and not characterized functionally. We generated *Hsf2bp* knockout mice and found a defect in meiotic HR leading to male infertility.

RESULTS

HSF2BP Is a Member of the BRCA Complex in mESCs

We previously described efficient immunoprecipitation of BRCA2-GFP and most of the known BRCA2-interacting proteins from *Brc2*^{GFP/GFP} knockin mouse embryonic stem cells (mESCs) (Reuter et al., 2014), and the phenomenon of BRCA2 degradation induced by mild hyperthermia (Krawczyk et al., 2011). With these at hand, we performed quantitative stable isotope labeling using amino acids in cell culture (SILAC)-based mass spectrometry experiments and identified HSF2BP as one of the proteins whose abundance in the BRCA2-GFP immunoprecipitate co-varies with that of BRCA2 upon hyperthermia treatment (Figure 1A). HSF2BP was previously described as a testis-specific, heat shock factor 2 (HSF2)-binding protein (Yoshima et al., 1998), and its association with BRCA2 or expression in tissues other than testis has not yet been reported. A reciprocal mass spectrometry experiment—GFP immunoprecipitation from *Hsf2bp*^{GFP/+} knockin mESCs—confirmed the interaction (Figure 1B). We used immunoprecipitation from *Rad51ap1*^{GFP/GFP} knockin cells (Figure 1B, x axis) as a control in these experiments to ensure that the interactions were not due to non-specific binding to nuclear GFP-tagged low-abundance DNA repair proteins (Modesti et al., 2007). The untagged

endogenous HSF2BP co-precipitated with HSF2BP-GFP produced from the knockin allele, which is indicative of oligomerization either between HSF2PB species or via the BRCA complex (Figure 1C). Furthermore, HSF2BP co-precipitated with PALB2, a localizer of BRCA2 (Xia et al., 2006) from *Palb2*^{GFP/GFP} knockin mESCs (Figure 1D).

HSF2BP-GFP in *Hsf2bp*^{GFP/+} cells was predominantly nuclear and localized to spontaneous and DNA damage-induced foci that are readily detectable without pre-extraction (Figure 1E). The foci colocalized with the DSB marker 53BP1 (78% partial or complete colocalization in the nuclei containing both HSF2BP and 53BP1 foci; SD 23%, n = 50) and were observed in the subpopulation of cells that was positive for the S-G2-M marker geminin (Figure 1F), as expected given that HR activity, and specifically BRCA2 expression in mESCs (Reuter et al., 2014), is confined to S and G2 phases of the cell cycle. We previously found, using oblique illumination microscopy and single-particle tracking, that endogenous GFP-tagged BRCA2 diffuses in oligomeric clusters that become immobilized upon the induction of DNA damage (Reuter et al., 2014). The same technique was applied to monitor and quantify HSF2BP-GFP diffusion in the nucleus, which revealed heterogeneous behavior very similar to that of BRCA2-GFP, including ionizing radiation-induced immobilization (Figure 1G). Taken together, the immunoprecipitation mass spectrometry and microscopy data suggest that HSF2BP and BRCA2 exist in a physiological complex in mESCs, which may be constitutive.

The interaction between HSF2BP and BRCA2 is evolutionarily conserved, as not only their human orthologs (Figure 1H) but also endogenous BRCA2 from the frog (*Xenopus laevis*) interacted efficiently with both recombinant *X. laevis* HSF2BP (xHSF2BP) and recombinant human HSF2BP (Figures 1I and 1J). This interaction did not affect the interaction of BRCA2 with RAD51 (Figures 1I and 1J). Such conservation is remarkable, given the evolutionary distance between the species, and indicates that the interaction is under strong selective pressure and therefore is functionally important.

Hsf2bp Inactivation Causes Meiotic HR Defect in Mouse Testis

Given the reported testis-specific expression (Yoshima et al., 1998) and our detection of HSF2BP in mESCs, we speculated that the protein may function in meiosis or early development. To investigate the physiological function, we engineered an *Hsf2bp*-deficient mouse strain by excising exons 3–6 using CRISPR/Cas9 in the zygote (Figures 2A and 2B). *Hsf2bp*^{−/−} animals were superficially normal; however, testis sizes were

(C) GFP colPs from indicated knockin mESCs analyzed by immunoblotting with the indicated antibodies. *Non-specific band.

(D) SILAC mass spectrometry of PALB2-GFP and RAD51AP1-GFP colP, plotted as in (B).

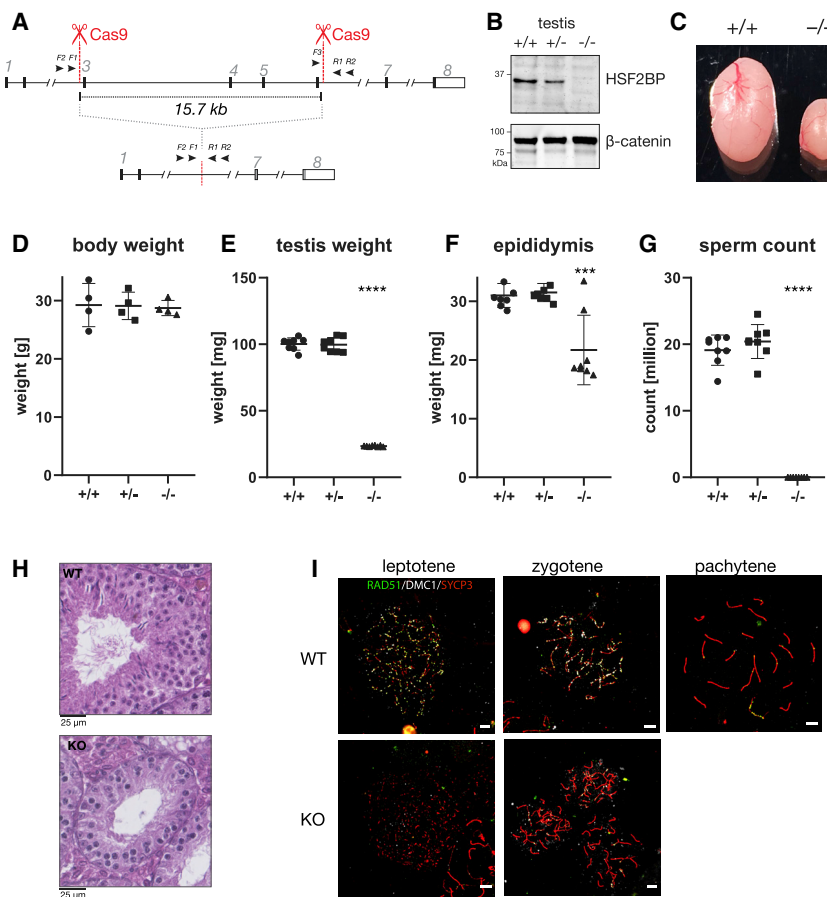
(E) Anti-53BP1 immunofluorescence microscopy of *Hsf2bp*^{GFP/GFP} and control cells treated with DNA-damaging agents; nuclei outlined based on DAPI, scale bar represents 5 μm.

(F) Anti-geminin immunofluorescence microscopy of *Hsf2bp*^{GFP/GFP} cells treated with or without MMC. Two representative nuclei (geminin[−] and geminin⁺) from MMC-treated cells, and HSF2BP foci quantification are shown (n = 2, lines indicate mean and SD).

(G) Duration of mobile and immobile states for single HSF2BP-GFP and BRCA2-GFP particles in live mESCs (control and irradiated) imaged by oblique illumination microscopy (n = 3).

(H) GFP colP from HEK293T cells producing GFP-HSF2BP (human or mouse) and MBP-BRCA2.

(I and J) CoIP of endogenous *X. laevis* BRCA2 and purified recombinant human (H; I) or *X. laevis* (X; J) HSF2BP from *Xenopus* egg extracts with or without recombinant HSF2BP added.



severely reduced, no sperm could be isolated from them (Figures 2C–2G), and no litters were produced from mating 9 different knockout males with wild-type females. Histological analysis revealed the absence of meiotic metaphases and post-meiotic cells and the frequent occurrence of aberrant spermatocytes in *Hsf2bp*^{−/−} testes (Figure 2H). Next, we performed immunofluorescent staining of *Hsf2bp*^{−/−} and control spermatocyte nuclei (Figures 2I and S1A). In leptotene, no specific RAD51 and DMC1 foci were observed, but zygotene nuclei contained a low and variable number of foci that colocalized on the partially synapsing chromosomes. Usually only 2–3 chromosome pairs appeared normally synapsed, but in some nuclei, the majority of chromosomes were normally synapsed (lower right nucleus in Figure 2I, 12 normal-looking synaptonemal complexes). In wild-type (WT) nuclei, numerous colocalizing RAD51 and DMC1 foci were observed in leptotene and zygotene nuclei, gradually decreasing in number as chromosome pairing progresses. In midpachytene, DMC1 foci had disappeared and some RAD51 foci remained prominent along the unsynapsed axes of the X chromosome. In *Hsf2bp*^{−/−} (knockout [KO]) nuclei, no pachytene were found.

These observations establish HSF2BP as a protein required for male meiosis, which is consistent with the initial description of HSF2BP as a testis-specific protein and its association with

Figure 2. Physiological Role of HSF2BP

(A) Schematic of mouse *Hsf2bp* locus depicting the location of Cas9 cuts used to produce the *Hsf2bp*^{−/−} null allele.

(B) Immunoblot confirming the disappearance of HSF2BP from the total testis lysates in the *Hsf2bp*^{−/−} mouse model.

(C–G) Representative image, displaying the strongly reduced testis size of *Hsf2bp*^{−/−} testis compared to wild-type control (C). Body weight (D), testis (E), and epididymis (F) weight, as well as sperm counts per epididymis (G) were compared between all 3 genotypes (15 weeks old, n = 4, lines indicate mean and SD).

(H) Representative histological images of testis cross-sections of wild-type (WT) and *Hsf2bp*^{−/−} (KO) 15-week-old mice.

(I) Spread spermatocyte nuclei immunostained with anti-RAD51, anti-DMC1 (meiotic DSB markers), and anti-SYCP3 (chromosomal axes and meiotic prophase stage marker), scale bar represents 5 μm.

BRCA2. Knockout females were fertile, and the reduction in litter sizes was not statistically significant in our cohort (*Hsf2bp*^{+/+}: n = 17, 133 pups, 6.6 per litter; *Hsf2bp*^{−/−}: n = 14, 79 pups, 5.6 per litter; p = 0.35, unpaired t test). Thus, the effect of HSF2BP deficiency on meiosis is less severe than the loss of BRCA2 (Sharan et al., 2004). In addition to the male infertility, *Hsf2bp*^{−/−} animals were born at a sub-mendelian frequency (numbers observed [expected] from *Hsf2bp*^{+/−} crosses: +/+: 38[36], +/−: 83[72], −/−: 23[36]; n = 27, χ^2 p = 0.039), suggesting an HSF2BP function in early development.

Hsf2bp Knockout Sensitizes ESCs to DNA Damage

To investigate the function of HSF2BP in ESCs, we created *Hsf2bp* knockout mESC lines using 2 different gene targeting strategies (Figures S1B–S1D). We tested their sensitivity to ionizing radiation and the DNA crosslinking agent mitomycin C (MMC) and measured the efficiency of HR by the *Rad54* gene targeting assay (Zelensky et al., 2013). While the efficiency of HR was not significantly different (Figure S1G), both HSF2BP-deficient cell lines showed increased sensitivity to ionizing radiation and MMC (Figures S1E and S1F). Overproduction of HSF2BP did not revert this phenotype, and in fact, it sensitized cells to ionizing radiation (IR) and MMC, which suggests that overproduction and loss of HSF2BP affects DNA repair in ESCs (Figures S1B, S1E, and S1F).

HSF2BP Is Expressed in Human Cancer Cells

Although in mice we only detected the HSF2BP protein in testis, we could readily detect HSF2BP transcripts by RT-PCR in all of the human cancer cell lines we tested (Figures S2A–S2C). Furthermore, inspection of public RNA expression datasets (Harding et al., 2011; Petryszak et al., 2016; Shin et al., 2011; Tang et al., 2017) indicated a high-level expression of HSF2BP,

not only in testis but also in mouse embryonic ovaries and human tumor samples derived from brain, breast, ovarian, and head and neck cancers (Figure S2D). This further supports the hypothesis that HSF2BP has roles outside spermatogenesis.

Mapping the BRCA2-HSF2BP Interaction

To identify the regions that are required for the interaction between BRCA2 and HSF2BP, we engineered a series of FLAG-tagged BRCA2 fragment expression constructs and GFP-tagged HSF2BP expression constructs (Figures 3A–3C). For BRCA2, starting by dividing the protein into 3 fragments (N-terminal, middle, and C-terminal) (Figure S3A), we mapped the HSF2BP-binding domain (HBD) to the 68-amino acid region (BRCA2-F9, Gly2270-Thr2337 in hBRCA2) located between the eighth BRC repeat (BRC8) and the DNA binding domain (Figure 3C). Despite the modest average conservation of the region between BRC8 and the DNA binding domain, the HBD is highly conserved and contains several amino acid motifs that are identical among vertebrate BRCA2 orthologs, including *X. laevis* (Figure S3B). Deletion of the corresponding region from full-length BRCA2 (BRCA2ΔF9) essentially abolished the interaction with HSF2BP (Figure 3C, lane 6), indicating that this is the only high-affinity interaction site.

Most of the GFP-fused truncated or internally deleted forms of HSF2BP we engineered were expressed at much lower levels than the full-length protein in human cells, presumably due to instability caused by misfolding (Figure 3C, lanes 8–10). However, we established that deletions of the central and C-terminal parts of HSF2BP, which are predicted to adopt the armadillo repeat folds (e.g., Phyre2; Kelley et al., 2015), abolished the interaction with BRCA2. Using internal deletions and, eventually, a set of 7 point mutants (Figure S3C), we determined that this region is required for interaction with BRCA2 and that a single amino acid change in HSF2BP at position 200 from arginine to threonine (R200T) greatly reduces its ability to co-precipitate BRCA2 (Figure 3C lanes 11–13) and abolishes localization of the GFP-tagged HSF2BP to repair foci (Figure S3D). Notably, this residue is fully conserved among vertebrates. We also established that the N-terminal 92 amino acids, which are not predicted to contain armadillo folds and show weak sequence similarity to coiled-coil regions, are not required for the interaction with BRCA2 (Figure 3C, lane 8).

To establish whether HSF2BP-BRCA2 interaction is direct, we purified bacterially expressed HSF2BP variants and BRCA2 fragments with tobacco etch virus (TEV)-cleavable 6xHis or glutathione S-transferase (GST) tags (Figure S3E). Full-length HSF2BP was retained by the GST-tagged BRCA2-F6 fragment immobilized on glutathione Sepharose beads, which demonstrated direct interaction between BRCA2 and HSF2BP. Consistent with the immunoprecipitation results, the purified HSF2BP R200T mutant did not bind BRCA2-F6 efficiently (Figure S3E). Moreover, analytical gel filtration of HSF2BP and the BRCA2-F8 fragment, re-purified after cleaving off affinity tags, confirmed the formation of a stable complex between the 2 proteins and the disruption of this complex in the presence of the HSF2BP R200T mutant (Figure 3D). The hydrodynamic volume of HSF2BP was severalfold higher than expected for a globular monomeric protein of its size (37.6 kDa), suggesting that HSF2BP exists in oligo-

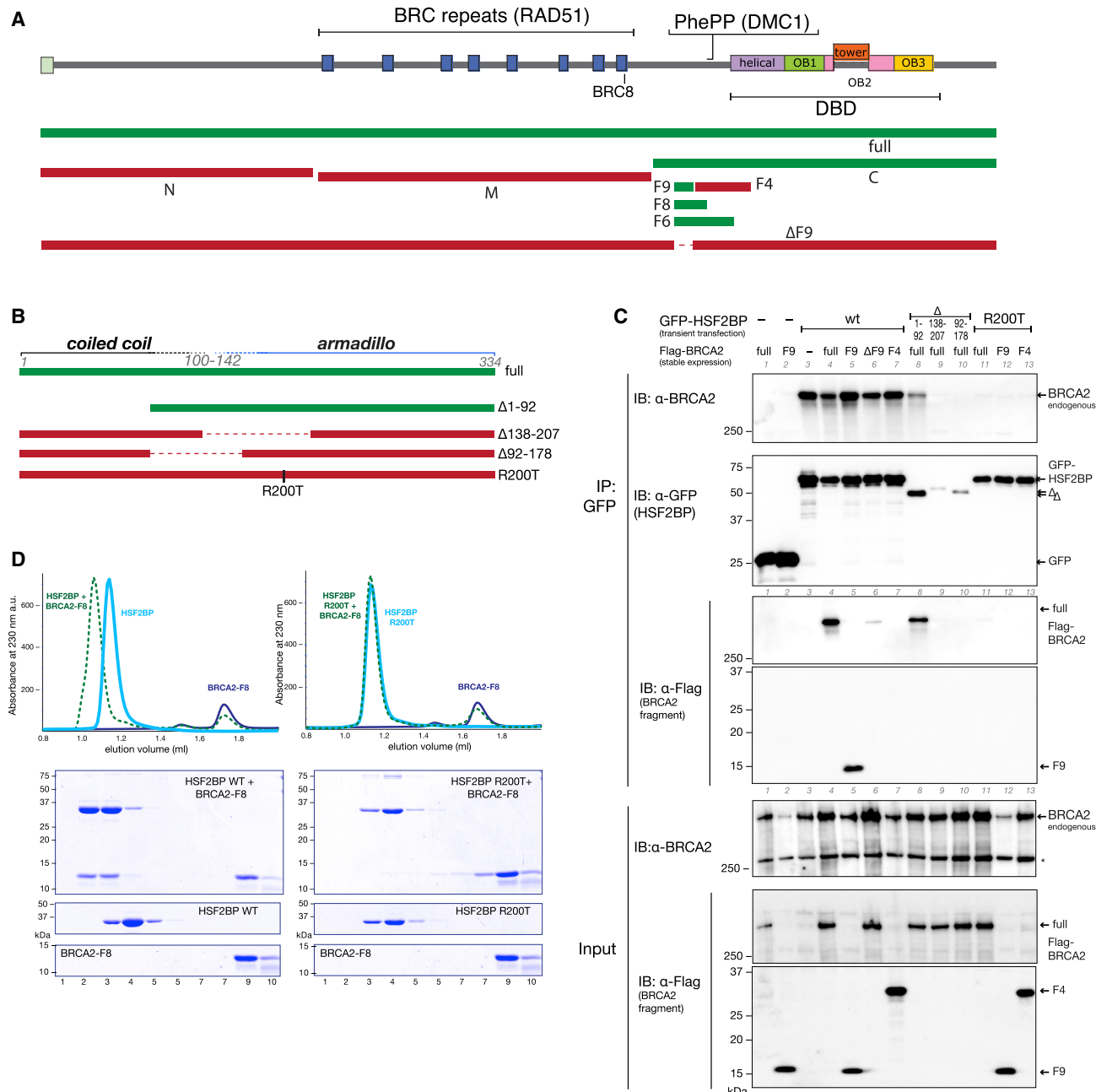
meric and/or elongated forms (Figure S3F), which is also consistent with the immunoprecipitation results (Figure 1C).

DISCUSSION

Our study reveals that BRCA2, a key mediator of HR in vertebrates, forms a direct and evolutionarily conserved interaction with a previously functionally uncharacterized protein HSF2BP. Consistent with the initial identification of HSF2BP as a testis-specific protein, we found that it is required for meiotic HR during spermatogenesis. Focal accumulation of RAD51 and DMC1 is delayed in the nuclei of spermatocytes from the *Hsf2bp*^{-/-} mice, and only a few foci were observed in the zygotene nuclei, suggesting their impaired formation or reduced stability or both. Chromosome synapsis was greatly impaired, but some normally synapsed chromosomes were visible in the late zygotene-like nuclei. This is consistent with the notion that at least some DSB sites can accumulate strand exchange proteins and be repaired in such a manner that they contribute to homology recognition and synapsis. However, overall, there is a severe chromosome pairing and meiotic DSB-repair defect in these mice, since no pachytene nuclei were observed.

Given the importance of BRCA2 for meiotic HR, it appears likely that the meiotic defect caused by the loss of HSF2BP involves BRCA2 interaction, and some evidence for this was reported independently (Zhang et al., 2019) while the present article was under review. However, even an incomplete loss of BRCA2 due to the inefficient expression of a “rescue” transgene in the germline of the *Brca2* knockout mouse leads to a more general meiotic defect, as oocyte meiosis was also affected, leading to female infertility (Sharan et al., 2004). This contrasts with the normal female fertility observed in our cohort and suggests that if HSF2BP exerts its role in meiosis via its interaction with BRCA2, only part of the essential BRCA2 function is dependent on it. Also noteworthy are spermatogenesis defects in mouse models deficient for the 2 transcription factors with which HSF2BP was previously reported to interact: HSF2 (Yoshima et al., 1998) and BNC1 (Wu et al., 2013). Loss of HSF2 in mice leads to meiotic defects in both spermatogenesis and oogenesis, although the effect on fertility (normal in males, reduced in females) is the opposite of what we observed in our *Hsf2bp*^{-/-} model (Kallio et al., 2002). *Bnc1* knockout mice, in addition to severe subfertility in both males and females, were born at sub-mendelian ratios (Zhang et al., 2012), which parallels our observations from *Hsf2bp*^{+/-} intercrosses. We hypothesized that the role of *Hsf2bp* in mESCs, where it is expressed at levels similar to testis and contributes to genome stability, may explain our observation; however, other mechanisms are possible. Further investigation of the molecular details, careful comparison of the phenotypes of the existing mouse models, and generation of the new ones (e.g., *Brca2* ΔHBD) will be required to answer these questions.

The *BRCA2* gene has been extensively sequenced to identify variants predisposing to breast cancer. We found no cancer-associated missense mutations in the HSF2BP-binding domain of BRCA2 in several curated databases (Béroud et al., 2016; Fokkema et al., 2011; Szabo et al., 2000). However, 2 variants (R2336H and I2285V) in this region and a naturally occurring

**Figure 3. Mapping of BRCA2-HSF2BP Interaction**

(A and B) Schematic of the BRCA2 (A) and HSF2BP (B) domain structure, fragments, and internal deletion variants used to determine interacting (green) and non-interacting (red) variants.

(C) GFP co-immunoprecipitation from HeLa cells stably expressing FLAG-tagged BRCA2 variants and transiently transfected with the indicated GFP-HSF2BP expression constructs (WT, full-length wild type, Δ, N-terminal and internal deletions, R200T point mutant).

(D) Interaction between purified untagged hHSF2BP and BRCA2-F8 fragments studied separately (solid lines) or after co-incubation (dotted lines) by analytical size exclusion chromatography. Complex formation between BRCA2-F8 and wild-type but not R200T mutant HSF2BP led to an increase in hydrodynamic radius and elution in earlier fractions.

alternative splicing event leading to skipping exon 12 encoding most of the HSF2BP-binding domain have been experimentally characterized. R2336H is classified as potentially deleterious or causal, but its effect is attributed to aberrant splicing and

BRCA2 protein truncation (Biswas et al., 2011; Claes et al., 2004). Skipping exon 12 does not lead to a reading frameshift and has no effect on *in vitro* BRCA2 functional assays (Bièche and Lidereau, 1999; Li et al., 2009; Rauh-Adelmann et al.,

2000). The second characterized polymorphism (I2285V, c.6853A > G) increases the frequency of exon 12 skipping and, in agreement with the *in vitro* data, is not associated with cancer predisposition (Li et al., 2009). The meiotic defect caused by *Hsf2bp* deficiency, its expression profile, the phenotype of knockout mESCs, and the details of BRCA2-HSF2BP interaction that we present here suggest that the highly conserved region of BRCA2 encoded by exons 12 and 13 has a function in meiosis rather than tumor suppression, and that polymorphisms in this region may affect fertility.

STAR★METHODS

Detailed methods are provided in the online version of this paper and include the following:

- KEY RESOURCES TABLE
- LEAD CONTACT AND MATERIALS AVAILABILITY
- EXPERIMENTAL MODEL AND SUBJECT DETAILS
 - Cell lines
 - Animals
- METHOD DETAILS
 - Generation of genetically modified cell lines
 - Mass spectrometry
 - Expression Constructs
 - Rad54 gene targeting assay
 - Clonogenic survivals
 - Antibodies and Immunoblotting
 - Protein Purification
 - Sequence and expression analysis
 - Analytical Gel Filtration
 - GST Pull-down
 - Immunoprecipitation (IP)
 - Immunofluorescence and Microscopy
 - *Hsf2bp* knockout mouse model
- QUANTIFICATION AND STATISTICAL ANALYSIS

SUPPLEMENTAL INFORMATION

Supplemental Information can be found online at <https://doi.org/10.1016/j.celrep.2019.05.096>.

ACKNOWLEDGMENTS

The authors would like to thank Dr. John Martens for help with the analysis of the expression data and G. Stier from the European Molecular Biology Laboratory (EMBL) for providing pETM11 and pETM30. K.S. was supported by the Uehara Memorial Foundation, the Mochida Memorial Foundation for Medical and Pharmaceutical Research, and the Japan Society for the Promotion of Science (JSPS) Postdoctoral Fellowship for Research Abroad. P.K. was supported by the Netherlands Organisation for Scientific Research (NWO) (VIDI 700.10.421) and a project grant from the Dutch Cancer Society (KWF HUBR 2015-7736). This research was funded by the Dutch Cancer Society and by the Gravitation Programme CancerGenomiCs.nl from the Netherlands Organisation for Scientific Research (NWO) and is part of the Oncode Institute, which is partly financed by the Dutch Cancer Society. The research leading to these results has received funding from the European Community's Seventh Framework Program (FP7/2007-2013) under grant agreement HEALTH-F2-2010-259893, the Dutch Cancer Society (grant EMCR 2008-4045), and a Ride for the Roses cancer research grant.

AUTHOR CONTRIBUTIONS

A.N.Z. and R.K. conceived the study. I.B., K.S., S.E.v.R.-F., M.R., H.O., N.v.d.T., and A.N.Z. performed the ESC and biochemical experiments. N.v.V., A.M., E.S., and A.N.Z. performed the mouse experiments. D.H.W.D. and K.B. collected the mass spectrometry data. J.A.A.D., J.L., C.W., J.E., D.C.v.G., W.M.B., P.K., A.N.Z., and R.K. supervised different parts of the study. A.N.Z., R.K., and P.K. wrote the manuscript, with contributions from the other authors. All of the authors read and approved the manuscript.

DECLARATION OF INTERESTS

The authors declare no competing interests.

Received: July 16, 2018

Revised: May 1, 2019

Accepted: May 23, 2019

Published: June 25, 2019

REFERENCES

- Abramoff, M.D., Magalhaes, P.J., and Ram, S.J. (2004). Image Processing with ImageJ. *Biophoton. Int.* 11, 36–42.
- Abreu, C.M., Prakash, R., Romanienko, P.J., Roig, I., Keeney, S., and Jasen, M. (2018). Shu complex SWS1-SWSAP1 promotes early steps in mouse meiotic recombination. *Nat. Commun.* 9, 3961.
- Adams, D.J., Quail, M.A., Cox, T., van der Weyden, L., Gorick, B.D., Su, Q., Chan, W.-I., Davies, R., Bonfield, J.K., Law, F., et al. (2005). A genome-wide, end-sequenced 129Sv BAC library resource for targeting vector construction. *Genomics* 86, 753–758.
- Alavattam, K.G., Kato, Y., Sin, H.-S., Maezawa, S., Kowalski, I.J., Zhang, F., Pang, Q., Andreassen, P.R., and Namekawa, S.H. (2016). Elucidation of the Fanconi Anemia Protein Network in Meiosis and Its Function in the Regulation of Histone Modifications. *Cell Rep.* 17, 1141–1157.
- Béroud, C., Letovsky, S.I., Braastad, C.D., Caputo, S.M., Beaudoux, O., Bignon, Y.-J., Bressac-De Paillerets, B., Bronner, M., Buell, C.M., Collod-Béroud, G., et al.; Laboratory Corporation of America Variant Classification Group; Quest Diagnostics Variant Classification Group; UNICANCER Genetic Group BRCA Laboratory Network (2016). BRCA Share: A Collection of Clinical BRCA Gene Variants. *Hum. Mutat.* 37, 1318–1328.
- Bièche, I., and Lidereau, R. (1999). Increased level of exon 12 alternatively spliced BRCA2 transcripts in tumor breast tissue compared with normal tissue. *Cancer Res.* 59, 2546–2550.
- Biswas, K., Das, R., Alter, B.P., Kuznetsov, S.G., Stauffer, S., North, S.L., Burkett, S., Brody, L.C., Meyer, S., Byrd, R.A., and Sharan, S.K. (2011). A comprehensive functional characterization of BRCA2 variants associated with Fanconi anemia using mouse ES cell-based assay. *Blood* 118, 2430–2442.
- Cadiñanos, J., and Bradley, A. (2007). Generation of an inducible and optimized piggyBac transposon system. *Nucleic Acids Res.* 35, e87.
- Carofiglio, F., Inagaki, A., de Vries, S., Wassenaar, E., Schoenmakers, S., Vermeulen, C., van Cappellen, W.A., Sleddens-Linkels, E., Grootegoed, J.A., Te Riele, H.P., et al. (2013). SPO11-independent DNA repair foci and their role in meiotic silencing. *PLoS Genet.* 9, e1003538.
- Chalkley, G.E., and Verrijzer, C.P. (2004). Immuno-depletion and purification strategies to study chromatin-remodeling factors *in vitro*. *Methods Enzymol.* 377, 421–442.
- Chen, P.L., Chen, C.F., Chen, Y., Xiao, J., Sharp, Z.D., and Lee, W.H. (1998). The BRC repeats in BRCA2 are critical for RAD51 binding and resistance to methyl methanesulfonate treatment. *Proc. Natl. Acad. Sci. USA* 95, 5287–5292.
- Claes, K., Poppe, B., Coene, I., Paepe, A.D., and Messiaen, L. (2004). BRCA1 and BRCA2 germline mutation spectrum and frequencies in Belgian breast/ovarian cancer families. *Br. J. Cancer* 90, 1244–1251.

- Cox, J., Matic, I., Hilger, M., Nagaraj, N., Selbach, M., Olsen, J.V., and Mann, M. (2009). A practical guide to the MaxQuant computational platform for SILAC-based quantitative proteomics. *Nat. Protoc.* 4, 698–705.
- Fokkema, I.F.A.C., Taschner, P.E.M., Schaafsma, G.C.P., Celli, J., Laros, J.F.J., and den Dunnen, J.T. (2011). LOVD v.2.0: the next generation in gene variant databases. *Hum. Mutat.* 32, 557–563.
- Gibson, D.G., Young, L., Chuang, R.-Y., Venter, J.C., Hutchison, C.A., 3rd, and Smith, H.O. (2009). Enzymatic assembly of DNA molecules up to several hundred kilobases. *Nat. Methods* 6, 343–345.
- Harding, S.D., Armit, C., Armstrong, J., Brennan, J., Cheng, Y., Haggarty, B., Houghton, D., Lloyd-MacGillip, S., Pi, X., Roochun, Y., et al. (2011). The GUDMAP database—an online resource for genitourinary research. *Development* 138, 2845–2853.
- Hooper, M., Hardy, K., Handyside, A., Hunter, S., and Monk, M. (1987). HPRT-deficient (Lesch-Nyhan) mouse embryos derived from germline colonization by cultured cells. *Nature* 326, 292–295.
- Inagaki, A., Schoenmakers, S., and Baarends, W.M. (2010). DNA double strand break repair, chromosome synapsis and transcriptional silencing in meiosis. *Epigenetics* 5, 255–266.
- Inano, S., Sato, K., Katsuki, Y., Kobayashi, W., Tanaka, H., Nakajima, K., Nakada, S., Miyoshi, H., Kries, K., Takaori-Kondo, A., et al. (2017). RFWD3-Mediated Ubiquitination Promotes Timely Removal of Both RPA and RAD51 from DNA Damage Sites to Facilitate Homologous Recombination. *Mol. Cell* 66, 622–634.e8.
- Jensen, R.B., Carreira, A., and Kowalczykowski, S.C. (2010). Purified human BRCA2 stimulates RAD51-mediated recombination. *Nature* 467, 678–683.
- Kallio, M., Chang, Y., Manuel, M., Alastalo, T.-P., Rallu, M., Gitton, Y., Pirkkala, L., Loones, M.-T., Paslaru, L., Larney, S., et al. (2002). Brain abnormalities, defective meiotic chromosome synapsis and female subfertility in HSF2 null mice. *EMBO J.* 21, 2591–2601.
- Kelley, L.A., Mezulis, S., Yates, C.M., Wass, M.N., and Sternberg, M.J. (2015). The Phyre2 web portal for protein modeling, prediction and analysis. *Nat. Protoc.* 10, 845–858.
- Klein Douwel, D., Boonen, R.A.C.M., Long, D.T., Szypowska, A.A., Räschle, M., Walter, J.C., and Knipscheer, P. (2014). XPF-ERCC1 acts in Unhooking DNA interstrand crosslinks in cooperation with FANCD2 and FANCP/SLX4. *Mol. Cell* 54, 460–471.
- Klovstad, M., Abdu, U., and Schüpbach, T. (2008). *Drosophila brca2* is required for mitotic and meiotic DNA repair and efficient activation of the meiotic recombination checkpoint. *PLoS Genet.* 4, e31.
- Knipscheer, P., Räschle, M., Smogorzewska, A., Enoui, M., Ho, T.V., Schärer, O.D., Elledge, S.J., and Walter, J.C. (2009). The Fanconi anemia pathway promotes replication-dependent DNA interstrand cross-link repair. *Science* 326, 1698–1701.
- Kojic, M., Kostrub, C.F., Buchman, A.R., and Holloman, W.K. (2002). BRCA2 homolog required for proficiency in DNA repair, recombination, and genome stability in *Ustilago maydis*. *Mol. Cell* 10, 683–691.
- Kottemann, M.C., and Smogorzewska, A. (2013). Fanconi anaemia and the repair of Watson and Crick DNA crosslinks. *Nature* 493, 356–363.
- Krawczyk, P.M., Eppink, B., Essers, J., Stap, J., Rodermond, H., Odijk, H., Zelensky, A.N., van Bree, C., Stalpers, L.J., Buist, M.R., et al. (2011). Mild hyperthermia inhibits homologous recombination, induces BRCA2 degradation, and sensitizes cancer cells to poly (ADP-ribose) polymerase-1 inhibition. *Proc. Natl. Acad. Sci. USA* 108, 9851–9856.
- Kuznetsov, S., Pellegrini, M., Shuda, K., Fernandez-Capetillo, O., Liu, Y., Martin, B.K., Burkett, S., Southon, E., Pati, D., Tessarollo, L., et al. (2007). RAD51C deficiency in mice results in early prophase I arrest in males and sister chromatid separation at metaphase II in females. *J. Cell Biol.* 176, 581–592.
- Li, L., Biswas, K., Habib, L.A., Kuznetsov, S.G., Hamel, N., Kirchhoff, T., Wong, N., Armel, S., Chong, G., Narod, S.A., et al. (2009). Functional redundancy of exon 12 of BRCA2 revealed by a comprehensive analysis of the c.6853A>G (p.I2285V) variant. *Hum. Mutat.* 30, 1543–1550.
- Lienert, F., Mohn, F., Tiwari, V.K., Baubec, T., Roloff, T.C., Gaidatzis, D., Stadler, M.B., and Schübeler, D. (2011). Genomic prevalence of heterochromatic H3K9me2 and transcription do not discriminate pluripotent from terminally differentiated cells. *PLoS Genet.* 7, e1002090.
- Mali, P., Yang, L., Esvelt, K.M., Aach, J., Güell, M., DiCarlo, J.E., Norville, J.E., and Church, G.M. (2013). RNA-guided human genome engineering via Cas9. *Science* 339, 823–826.
- Martinez, J.S., Baldeyron, C., and Carreira, A. (2015). Molding BRCA2 function through its interacting partners. *Cell Cycle* 14, 3389–3395.
- Martinez, J.S., von Nicolai, C., Kim, T., Ehlin, Å., Mazin, A.V., Kowalczykowski, S.C., and Carreira, A. (2016). BRCA2 regulates DMC1-mediated recombination through the BRC repeats. *Proc. Natl. Acad. Sci. USA* 113, 3515–3520.
- Meuwissen, R.L., Offenberg, H.H., Dietrich, A.J., Riesewijk, A., van Iersel, M., and Heyting, C. (1992). A coiled-coil related protein specific for synapsed regions of meiotic prophase chromosomes. *EMBO J.* 11, 5091–5100.
- Modesti, M., Budzowska, M., Baldeyron, C., Demmers, J.A.A., Ghirlando, R., and Kanaar, R. (2007). RAD51AP1 is a structure-specific DNA binding protein that stimulates joint molecule formation during RAD51-mediated homologous recombination. *Mol. Cell* 28, 468–481.
- Pellegrini, L., Yu, D.S., Lo, T., Anand, S., Lee, M., Blundell, T.L., and Venkitaraman, A.R. (2002). Insights into DNA recombination from the structure of a RAD51-BRCA2 complex. *Nature* 420, 287–293.
- Peters, A.H., Plug, A.W., van Vugt, M.J., and de Boer, P. (1997). A drying-down technique for the spreading of mammalian meiocytes from the male and female germline. *Chromosome Res.* 5, 66–68.
- Petryszak, R., Keays, M., Tang, Y.A., Fonseca, N.A., Barrera, E., Burdett, T., Füllgrabe, A., Fuentes, A.M.-P., Jupp, S., Koskinen, S., et al. (2016). Expression Atlas update—an integrated database of gene and protein expression in humans, animals and plants. *Nucleic Acids Res.* 44 (D1), D746–D752.
- Potter, S.C., Luciani, A., Eddy, S.R., Park, Y., Lopez, R., and Finn, R.D. (2018). HHMMer web server: 2018 update. *Nucleic Acids Res.* 46 (W1), W200–W204.
- Prakash, R., Zhang, Y., Feng, W., and Jasin, M. (2015). Homologous recombination and human health: the roles of BRCA1, BRCA2, and associated proteins. *Cold Spring Harb. Perspect. Biol.* 7, a016600.
- Ran, F.A., Hsu, P.D., Wright, J., Agarwala, V., Scott, D.A., and Zhang, F. (2013). Genome engineering using the CRISPR-Cas9 system. *Nat. Protoc.* 8, 2281–2308.
- Rauh-Apelmann, C., Lau, K.M., Sabeti, N., Long, J.P., Mok, S.C., and Ho, S.M. (2000). Altered expression of BRCA1, BRCA2, and a newly identified BRCA2 exon 12 deletion variant in malignant human ovarian, prostate, and breast cancer cell lines. *Mol. Carcinog.* 28, 236–246.
- Reuter, M., Zelensky, A., Smal, I., Meijering, E., van Cappellen, W.A., de Gruiter, H.M., van Belle, G.J., van Royen, M.E., Houtsmuller, A.B., Essers, J., et al. (2014). BRCA2 diffuses as oligomeric clusters with RAD51 and changes mobility after DNA damage in live cells. *J. Cell Biol.* 207, 599–613.
- Robert, T., Nore, A., Brun, C., Maffre, C., Crimi, B., Bourbon, H.-M., and de Massy, B. (2016). The TopoVIB-Like protein family is required for meiotic DNA double-strand break formation. *Science* 351, 943–949.
- Roy, R., Chun, J., and Powell, S.N. (2011). BRCA1 and BRCA2: different roles in a common pathway of genome protection. *Nat. Rev. Cancer* 12, 68–78.
- Seeliger, K., Dukovic-Schulze, S., Wurz-Wildersinn, R., Pacher, M., and Puchta, H. (2012). BRCA2 is a mediator of RAD51- and DMC1-facilitated homologous recombination in *Arabidopsis thaliana*. *New Phytol.* 193, 364–375.
- Sharan, S.K., Morimatsu, M., Albrecht, U., Lim, D.S., Regel, E., Dinh, C., Sands, A., Eichle, G., Hasty, P., and Bradley, A. (1997). Embryonic lethality and radiation hypersensitivity mediated by Rad51 in mice lacking Brca2. *Nature* 386, 804–810.
- Sharan, S.K., Pyle, A., Coppola, V., Babus, J., Swaminathan, S., Benedict, J., Swing, D., Martin, B.K., Tessarollo, L., Evans, J.P., et al. (2004). BRCA2 deficiency in mice leads to meiotic impairment and infertility. *Development* 131, 131–142.

- Shin, G., Kang, T.-W., Yang, S., Baek, S.-J., Jeong, Y.-S., and Kim, S.-Y. (2011). GENT: gene expression database of normal and tumor tissues. *Cancer Inform.* 10, 149–157.
- Siaud, N., Dray, E., Gy, I., Gérard, E., Takvorian, N., and Doutriaux, M.-P. (2004). Brca2 is involved in meiosis in *Arabidopsis thaliana* as suggested by its interaction with Dmc1. *EMBO J.* 23, 1392–1401.
- Simhadri, S., Peterson, S., Patel, D.S., Huo, Y., Cai, H., Bowman-Colin, C., Miller, S., Ludwig, T., Ganesan, S., Bhaumik, M., et al. (2014). Male fertility defect associated with disrupted BRCA1-PALB2 interaction in mice. *J. Biol. Chem.* 289, 24617–24629.
- Skarnes, W.C., Rosen, B., West, A.P., Koutsourakis, M., Bushell, W., Iyer, V., Mujica, A.O., Thomas, M., Harrow, J., Cox, T., et al. (2011). A conditional knockout resource for the genome-wide study of mouse gene function. *Nature* 474, 337–342.
- Szabo, C., Masiello, A., Ryan, J.F., and Brody, L.C. (2000). The breast cancer information core: database design, structure, and scope. *Hum. Mutat.* 16, 123–131.
- Tan, T.L., Essers, J., Citterio, E., Swagemakers, S.M., de Wit, J., Benson, F.E., Hoeijmakers, J.H., and Kanaar, R. (1999). Mouse Rad54 affects DNA conformation and DNA-damage-induced Rad51 foci formation. *Curr. Biol.* 9, 325–328.
- Tang, Z., Li, C., Kang, B., Gao, G., Li, C., and Zhang, Z. (2017). GEPIA: a web server for cancer and normal gene expression profiling and interactive analyses. *Nucleic Acids Res.* 45 (W1), W98–W102.
- Thorslund, T., Esashi, F., and West, S.C. (2007). Interactions between human BRCA2 protein and the meiosis-specific recombinase DMC1. *EMBO J.* 26, 2915–2922.
- Wamstad, J.A., Alexander, J.M., Truty, R.M., Shrikumar, A., Li, F., Eilertson, K.E., Ding, H., Wylye, J.N., Pico, A.R., Capra, J.A., et al. (2012). Dynamic and coordinated epigenetic regulation of developmental transitions in the cardiac lineage. *Cell* 151, 206–220.
- Wojtasz, L., Daniel, K., Roig, I., Bolcun-Filas, E., Xu, H., Boonsanay, V., Eckmann, C.R., Cooke, H.J., Jasim, M., Keeney, S., et al. (2009). Mouse HORMAD1 and HORMAD2, two conserved meiotic chromosomal proteins, are depleted from synapsed chromosome axes with the help of TRIP13 AAA-ATPase. *PLoS Genet.* 5, e1000702.
- Wong, A.K., Pero, R., Ormonde, P.A., Tavtigian, S.V., and Bartel, P.L. (1997). RAD51 interacts with the evolutionarily conserved BRC motifs in the human breast cancer susceptibility gene brca2. *J. Biol. Chem.* 272, 31941–31944.
- Wu, Y., Liao, S., Wang, X., Wang, S., Wang, M., and Han, C. (2013). HSF2BP represses BNC1 transcriptional activity by sequestering BNC1 to the cytoplasm. *FEBS Lett.* 587, 2099–2104.
- Xia, B., Sheng, Q., Nakanishi, K., Ohashi, A., Wu, J., Christ, N., Liu, X., Jasim, M., Couch, F.J., and Livingston, D.M. (2006). Control of BRCA2 cellular and clinical functions by a nuclear partner, PALB2. *Mol. Cell* 22, 719–729.
- Xu, X., Aprelikova, O., Moens, P., Deng, C.-X., and Furth, P.A. (2003). Impaired meiotic DNA-damage repair and lack of crossing-over during spermatogenesis in BRCA1 full-length isoform deficient mice. *Development* 130, 2001–2012.
- Yoshima, T., Yura, T., and Yanagi, H. (1998). Novel testis-specific protein that interacts with heat shock factor 2. *Gene* 214, 139–146.
- Yusa, K., Zhou, L., Li, M.A., Bradley, A., and Craig, N.L. (2011). A hyperactive piggyBac transposase for mammalian applications. *Proc. Natl. Acad. Sci. USA* 108, 1531–1536.
- Zelensky, A.N., Sanchez, H., Ristic, D., Vidic, I., van Rossum-Fikkert, S.E., Essers, J., Wyman, C., and Kanaar, R. (2013). Caffeine suppresses homologous recombination through interference with RAD51-mediated joint molecule formation. *Nucleic Acids Res.* 41, 6475–6489.
- Zelensky, A., Kanaar, R., and Wyman, C. (2014). Mediators of homologous DNA pairing. *Cold Spring Harb. Perspect. Biol.* 6, a016451.
- Zelensky, A.N., Schimmel, J., Kool, H., Kanaar, R., and Tijsterman, M. (2017). Inactivation of Pol θ and C-NHEJ eliminates off-target integration of exogenous DNA. *Nat. Commun.* 8, 66.
- Zhang, X., Chou, W., Haig-Ladewig, L., Zeng, W., Cao, W., Gerton, G., Dobrinski, I., and Tseng, H. (2012). BNC1 is required for maintaining mouse spermatogenesis. *Genesis* 50, 517–524.
- Zhang, J., Fujiwara, Y., Yamamoto, S., and Shibuya, H. (2019). A meiosis-specific BRCA2 binding protein recruits recombinases to DNA double-strand breaks to ensure homologous recombination. *Nat. Commun.* 10, 722.
- Zickler, D., and Kleckner, N. (2015). Recombination, Pairing, and Synapsis of Homologs during Meiosis. *Cold Spring Harb. Perspect. Biol.* 7, a016626.

STAR★METHODS

KEY RESOURCES TABLE

REAGENT or RESOURCE	SOURCE	IDENTIFIER
Antibodies		
RAD51	(Tan et al., 1999)	2307
BRCA2 Ab-1	Millipore	Cat# OP95; RRID:AB_2067762
FLAG M2	Sigma	Cat# F3165; RRID:AB_259529
DMC1	Abcam	Cat# ab11054; RRID:AB_297706
6xHis tag	Abcam	Cat# ab18184; RRID:AB_444306
GFP (clones 7.1 and 13.1)	Roche/Sigma	Cat# 11814460001; RRID:AB_390913
SYCP3	R&D systems	Cat# AF3750; RRID:AB_2197194
SYCP1	(Meuwissen et al., 1992)	N/A
HORMAD1	(Wojtasz et al., 2009)	N/A
HSF2BP	this paper	SY8126
HSF2BP	this paper	SY8127
BRCA2 raised against residues 1842-2080 of xIBRCA2	this paper	N/A
β-Catenin	BD Biosciences	Cat# 610153; RRID:AB_397554
53BP1	Novus Biologicals	Cat# NB100-304; RRID:AB_10003037
Geminin	Proteintech	Cat# 10802-I-AP; RRID:AB_2110945
Bacterial and Virus Strains		
<i>E. coli</i> : Rosetta2 (DE3) pLysS	Novagen	71403
Chemicals, Peptides, and Recombinant Proteins		
Protein: HSF2BP human	this paper	N/A
Protein: S.p. Cas9 3NLS	IDT	Cat# 1074181
Protein: His-GST-BRCA2-F6 (Gly2270–Asp2479)	this paper	N/A
Protein: BRCA2-F8 (Gly2270-Ala2351)	this paper	N/A
Anti-GFP agarose beads	Chromotek	Cat# gta-20
Protein A Sepharose Fast Flow beads	GE Healthcare	Cat# 17127901
Mitomycin C (MMC)	Sigma	Cat# M4287
Talazoparib (BMN 673)	Axon Medchem	Cat# 2502
Laminin	Roche	Cat# 11243217001
Experimental Models: Cell Lines		
IB10 (a subclone of E14 129/Ola) mouse ES cells	(Hooper et al., 1987)	N/A
<i>Brca2</i> ^{GFP/GFP} mouse ES cells	(Reuter et al., 2014)	N/A
<i>Hsf2bp</i> ^{GFP/+} mouse ES cells	this paper	N/A
<i>Hsf2bp</i> ^{GFP/GFP} mouse ES cells	this paper	N/A
<i>Rad51ap1</i> ^{GFP/GFP} mouse ES cells	this paper	N/A
<i>Hsf2bp</i> ^{ko/koNC} mouse ES cells	this paper	N/A
<i>Hsf2bp</i> ^{ko2/ko2} mouse ES cells	this paper	N/A
<i>Palb2</i> ^{GFP/GFP} mouse ES cells	this paper	N/A
Experimental Models: Organisms/Strains		
Mouse: C57BL/6 OlaHsd	Envigo	Cat# 057
Mouse: <i>Hsf2bp</i> ^{−/−}	this paper	N/A
Oligonucleotides		
Primer: hHSF2BP-rt-F1 cgcaaattctggagggtt	this paper	N/A
Primer: hHSF2BP-rt-R1 gatctggggagaaggcac	this paper	N/A
Primer: hHSF2BPDArm-R ggccttgacgacttcctcac	this paper	N/A

(Continued on next page)

Continued

REAGENT or RESOURCE	SOURCE	IDENTIFIER
Primer: hHSF2bpDC-F ccattttggaggagataaaagcttgaag	this paper	N/A
Primer: mHSF2BP-rt-F1 agctgaggcagcgctat	this paper	N/A
Primer: mHSF2BP-rt-R1 gatggaccactggcatttc	this paper	N/A
Primer: mHSF2BP-geno-F1 actacccctcaactgttagcat	this paper	N/A
Primer: mHSF2BP-geno-F2 gccagctgctctctttagt	this paper	N/A
Primer: mHSF2BP-geno-F3 tggctgtgaattcttgtga	this paper	N/A
Primer: mHSF2BP-geno-R1 tcatccggggccactgttaa	this paper	N/A
Primer: mHSF2BP-geno-R2 atgcataccgcgcacacaa	this paper	N/A
Recombinant DNA		
Plasmid: pGb-LPL-CAG → GFP-hHSF2BP	this paper	pAZ229
Plasmid: pGb-LPL-CAG → GFP-hHSF2BP R200T	this paper	pAZ284
Plasmid: pEGFPN1+mHSF2BP	this paper	pAZ022
Plasmid: pETM11+hHSF2BP	this paper	pAZ018
Plasmid: pETM30+BRCA2-F6 (Gly2270-Asp2479)	this paper	N/A
Plasmid: pETM11+BRCA2-F8 (Gly2270-Ala2351)	this paper	N/A
Plasmid: pETDuet-1+xhHSF2BP	this paper	N/A
Plasmid: pX459 V2.0	(Ran et al., 2013)	Addgene Plasmid #62988; RRID:Addgene_62988
Plasmid: pX459+Hsf2bp-GFP sgRNA	this paper	pAZ307
Plasmid: pBS+Hsf2bp-GFP donor	this paper	pAZ207
Plasmid: p15A+Hsf2bp-Ce3-BSD-neo ko1 donor	this paper	pAZ092
Plasmid: pBS+Hsf2bp-e2Δ-hygro ko2 donor	this paper	pAZ120
Plasmid: pCR-BluntII Hsf2bp e1 gRNA	this paper	pAZ074
Plasmid: pCR-BluntII Hsf2bp e2 gRNA	this paper	pAZ058
Plasmid: pCDNA3.3 Topo+Cas9	(Mali et al., 2013)	Addgene Plasmid #41815; RRID:Addgene_41815
Plasmid: gRNA cloning vector	(Mali et al., 2013)	Addgene Plasmid #41824; RRID:Addgene_41824
Plasmid: pBS+Palb2-CGN targeting construct	this paper	pAZ209
Plasmid: pX459+Palb2 gRNA last exon	this paper	pAZ206
Plasmid: pBS+Rad51ap1-CGN targeting construct	this paper	pAZ311
Plasmid: mPB (Cadiñanos and Bradley, 2007)	Sanger Institute Archives	N/A
Plasmid: pCMV-hyPBase (Yusa et al., 2011)	Sanger Institute Archives	N/A
Plasmid: pGb-LNL-CAG	(Zelensky et al., 2017)	pAZ125
Plasmid: pGb-LPL-CAG → Flag-BRCA2	this paper	pAZ148
Plasmid: pGb-LPL-CAG → Flag-BRCA2ΔF9	this paper	pAZ304
Plasmid: phCMV-MBPx2-BRCA2	(Jensen et al., 2010)	N/A
Software and Algorithms		
Prism	Graphpad	RRID:SCR_002798
ImageJ	(Abramoff et al., 2004)	RRID: SCR_003070
Single particle tracking plugin	(Reuter et al., 2014)	N/A
MATLAB	MathWorks	RRID: SCR_001622
MATLAB track analysis script	(Reuter et al., 2014)	N/A
Hmmsearch	(Potter et al., 2018)	N/A

LEAD CONTACT AND MATERIALS AVAILABILITY

Further information and requests for resources and reagents should be directed to and will be fulfilled by Alex N. Zelensky (a.zelensky@erasmusmc.nl). Distribution of the *Hsf2bp* knockout strain is subject to a material transfer agreement.

EXPERIMENTAL MODEL AND SUBJECT DETAILS

Cell lines

mES cell lines were derived from the IB10 cell line, which is a subclone of E14 129/Ola from male origin (Hooper et al., 1987), specific pathogen free. Cells were cultured on gelatinized plastic dishes (0.1% gelatin in water) as described before (Zelensky et al., 2017) at atmospheric oxygen concentration in media comprising 1:1 mixture of DMEM (Lonza BioWhittaker Cat. BE12-604F/U1, with Ultra-glutamine 1, 4.5 g/l Glucose) and BRL-conditioned DMEM, supplemented with 1000 U/ml leukemia inhibitory factor, 10% FCS, 1x NEAA, 200 U/ml penicillin, 200 µg/ml streptomycin, 89 µM β-mercaptoethanol. HeLa (human cervical adenocarcinoma, female origin) and HEK293T (human embryonic kidney, female origin) cells were cultured in DMEM supplemented with 10% FCS, 200 U/ml penicillin, 200 µg/ml streptomycin.

Animals

All animals were kept in accordance with local regulations under the work protocol 17-867-11. Animal experiments were approved by the Dutch competent authority (Centrale Commissie Dierproeven, CCD) and all experiments conform to relevant regulatory standards. Female mice for CRISPR/Cas9 injection were C57BL/6 OlaHsd from Envigo, age 5 weeks. For spermatogenesis defect analysis male mice were sacrificed at the age of 15 weeks. Female mouse fertility was assessed at the ages 9–28 weeks.

METHOD DETAILS

Generation of genetically modified cell lines

Hsf2bp^{GFP/+} mES cells were created by gene targeting using the approach we used previously to engineer the BRCA2-GFP knock-in lines (Reuter et al., 2014). The gene targeting construct was engineered by recombineering, starting with the BAC clone bMQ-430H02 from the Sanger 129/Sv library (Adams et al., 2005), homology arms were 3.1 and 6.2 kb long, and the GFP-2A-neo cassette was inserted after the last codon of the *Hsf2bp* CDS. After the completion of selection with 200 µg/ml G418 (Invivogen) clones were isolated. Correct targeting was confirmed by Southern blotting on HindIII-digested genomic DNA with an external probe. Two out of the 14 screened clones were identified as correctly recombined. *Hsf2bp*^{GFP/GFP} cells were produced using same targeting construct with CRISPR/Cas9 stimulation. The target for sgRNA cloned into pX459 vector (Ran et al., 2013), a gift from Feng Zhang (Addgene plasmid # 62988 ; <http://addgene:62988> ; RRID:Addgene_62988), was 5'-acatcttaaacattacagtcc-3'. Seven independent *Hsf2bp*^{GFP/GFP} clones were isolated. *Rad51ap1*^{wt/GFP} cells were produced by similar gene targeting procedure (BAC bMQ-338B20, 3.6 and 4.8 kb homology arms, resulting construct pAZ311) and converted to homozygosity by high-G418 selection as described before (Reuter et al., 2014) to generate the *Rad51ap1*^{GFP/GFP} line that was used as a control in the mass spectrometry experiments. The gene targeting construct for the production of *Palb2*^{GFP/GFP} cells was engineered using the same approach (BAC bMQ-128G09, 3.7 kb and 4.4 kb right homology arms, pAZ209) with Cas9 stimulation; the target for sgRNA cloned into pX459 was 5'-tatataccgatactttaaag-3' (pAZ206). One line of *Hsf2bp* knockout ES cells (ko1) was produced by sequential gene targeting and site-specific recombination steps using the knockout-first gene trap strategy (Skarnes et al., 2011) without CRISPR/Cas9 stimulation. Selection cassettes were removed using two rounds of site-specific recombination, as shown in Figure S1C, followed by re-targeting of the second allele with the same gene targeting construct, and excision of exon 3 using Cre/LoxP recombination; two independent clones were isolated in the first round of targeting and converted to homozygous knockout using the described procedure. The second line of *Hsf2bp* knockout ES cells was produced by CRISPR/Cas9-stimulated replacement of the first two exons and (part of) the promoter region (358 bp upstream of the start codon) with a hygromycin resistance gene under the human phosphoglycerate kinase (PGK) promoter. The gene targeting construct (pAZ120) contained 0.9 and 10.4 homology arms. The targets of the two gRNAs cloned into gRNA cloning vector (Mali et al., 2013), a gift from George Church (Addgene plasmid # 41824 ; <http://addgene:41824> ; RRID:Addgene_41824), were in exons 1 and 2 with target sequences gccccatggcccaaccgt and ggaccttggaaacggctgacga, respectively (constructs pAZ074 and pAZ058). The gene targeting construct, two gRNA expression constructs and the Cas9 expression construct (Addgene plasmid # 41815 ; <http://addgene:41815> ; RRID:Addgene_41815) were co-transfected by electroporation into IB10 cells (15 µg each plasmid DNA, 2–3×10⁷ cells); colonies were picked after 8 days of selection with 200 µg/ml hygromycin B (Roche, 10843555001). Clones with the homozygous loss of the wild-type allele were identified by genotyping PCRs and confirmed by immunoblotting; five independent clones were isolated. Further details of the gene targeting procedures and DNA constructs can be provided upon request.

With the exception of U2OS GFP-HSF2BP clone #5, all stable cell lines were constructed using PiggyBac vectors by co-transfecting them with the transposase expression construct (mPB (Cadiñanos and Bradley, 2007) or hyPBase (Yusa et al., 2011)), followed by selection with either 1.5 µg/ml puromycin or 800 µg/ml G418 was started and maintained for 6–10 days. Stable transformation was highly efficient (> 95% GFP+ cells when GFP-tagged constructs were used) and therefore clonal isolation was not performed.

Mass spectrometry

Stable isotope labeling in cell culture (SILAC) of mES cells was performed by expanding the cell lines from 6 cm to 2x 145mm dishes (gelatinized) in drop-out ES media (Mouse Stem Cell Expansion DMEM for SILAC, (#88207 Thermo Fisher) to which 3.5 mg/ml D-glucose, 105 µg/ml L-leucine, 50 mL dialyzed FCS, 6 mL ultraglutamine (Lonza BE17-605E/U1) were added) complemented with 84 µg/ml L-lysine (K) and 146 µg/ml L-arginine (R). Lysine and arginine differed in N and C isotopic content for three SILAC

states: K0R0 for light, K3R6 for medium and K8R10 for “heavy”; heavy-isotope amino acids were purchased from Cambridge Isotope Laboratories. Sample preparation after pull-down with anti-GFP nanobody agarose beads (Chromotek) involved either PAGE fractionation or on-beads digestion, followed by HPLC. Data acquisition was performed using LTQ-Orbitrap XL instrument (Thermo) and analyzed using MaxQuant software (Cox et al., 2009). In SILAC experiments involving hyperthermia treatment of *Brca2*^{GFP/GFP} mES cells, two label-swapped replicates were performed. One SILAC state in each replicate corresponds to 1 h incubation at 42°C (after 15 min pre-warming), which causes BRCA2 degradation (Krawczyk et al., 2011), the other to 37°C control. Normalized SILAC ratios were plotted.

Analysis of proteins co-immunoprecipitated by GFP beads with HSF2BP-GFP and RAD51AP1-GFP was performed in two separate experiments. Combined peptide intensities (Log10-transformed) were plotted. Missing intensity values representing proteins detected in only one immunoprecipitate were replaced with values imputed from normal distribution with a downshift of 3 for visualization purpose only; their ranges are demarcated with dotted lines on the plot. GFP co-immunoprecipitates from *Palb2*^{GFP/GFP} and *Rad51ap1*^{GFP/GFP} knock-in mES cells was performed after SILAC labeling (H and L states, respectively). Log10 intensity values were plotted, missing values were imputed as described above.

Expression Constructs

The CDS of human and mouse HSF2BP were PCR-amplified from first-strand cDNA synthesized from total RNA isolated from U2OS and mES IB10 cells, respectively, with SuperScript II enzyme (Invitrogen) and oligo-dT primer. The PCR products were cloned into pCR4 topo-TA vector (Invitrogen) and verified by Sanger sequencing. Clones containing sequences corresponding to the predicted full-length HSF2BP CDS as annotated the NCBI GenBank database (NM_007031 and NM_028902) were used as templates for sub-cloning. Re-cloning into destination vector was performed using isothermal Gibson assembly (Gibson et al., 2009). The GFP expression constructs used in the initial experiments were derived from pEGFP-N1 and pEGFP-C1 vectors for C- and N-terminal fusions, respectively. Other GFP- and Flag- tagged expression constructs were assembled in PiggyBac described before (pAZ125 (Zelensky et al., 2017)) or engineered using analogous steps in our lab. The PiggyBac vectors carried PGK-neo or PGK-puro selection cassettes and CAG promotor-driven transgene as a separate expression unit. Human BRCA2 CDS fragment were PCR-amplified or excised using restriction from phCMV-MBPx2-BRCA2 vector (Jensen et al., 2010) and cloned. All cloning junctions and fragments produced by PCR were sequence-verified after cloning. Internal deletion constructs, such as Flag-BRCA2ΔF9 (pAZ304), were produced by excising a fragment of full-length Flag-BRCA2 PiggyBac expression construct (pAZ148) using two unique restriction sites nearest to the region targeted for deletion and patching the gap with appropriate PCR-amplified fragment(s) encoding the desired deletion using Gibson assembly. Site-directed mutagenesis of GFP-HSF2BP was performed by amplifying two overlapping fragments with the mutation encoded by the overlapping part of the primers (20–25 bp) and cloning the two fragments into destination GFP PiggyBac vector. Proofreading Q5 PCR polymerase (NEB) was used and clones were verified by Sanger sequencing. Details of the PCR primers and cloning strategies are available upon request.

Rad54 gene targeting assay

Rad54-GFP gene targeting assay was performed as previously described (Zelensky et al., 2013): 6–12 million ES cells were electro-porated with Pvul-linearized Rad54-GFP gene targeting construct and seeded in 10 cm dish. Next day media was replaced to start selection with 1.5 µg/ml puromycin, and again on days 2 and 4. After colonies formed on day 6–8, cells were trypsinized, collected by centrifugation, re-suspended in 1 mL 1% PFA in PBS, incubated for 15 min to fix, diluted 1:1 in PBS 0.2% Triton X-100 and analyzed by FACS.

Clonogenic survivals

Before the experiment cells were maintained in 6-well plates and passaged at 5×10⁵ per well every two days. The baseline seeding density was 200 cells per well of a 6-well plate, it was increased to account for reduced plating efficiency at higher doses of damage. At least three independent experiments were performed in 6-well plates, each with technical triplicates. On day 1 cells were trypsinized, counted using Countess II automated cell counter (Thermo Fisher), a suspension with maximum concentration required for the experiment was prepared (usually 10,000 viable cells per ml, for 100x the number of cells seeded in the untreated wells), and serially diluted to produce lower concentrations (10x, 4x and 1x). The suspensions were then distributed at 2 mL per well into gelatinized 6-well plates (seeding densities: 4x for 2 Gy, 10x for 5 Gy, 100x for 8 Gy IR; 1x for 0.2 µg/ml, 4x for 0.3 and 0.4 µg/ml MMC). Next day plates were irradiated using RS320 X-ray source (Xstrahl) or treated with MMC for 2 h; at the end of MMC treatment media was removed, cells were washed with PBS, and 2 mL of fresh media was added. After six days media was aspirated, wells were rinsed with PBS and stained with Coomassie Brilliant Blue R (0.25% in 40% methanol, 10% acetic acid). Plates were photographed and macroscopically visible colonies were counted.

Antibodies and Immunoblotting

Antibodies used in this study were against RAD51 (rabbit 2307 (Tan et al., 1999)), BRCA2 (Ab-1, OP95, Millipore, RRID:AB_2067762, 1:1000), FLAG (M2 antibody, Sigma, F3165, RRID:AB_259529, 1:2500), GFP (clones 7.1 and 13.1, Roche, RRID:AB_390913, 1:1000–1:5000), β-catenin (BD Biosciences, 610153, RRID:AB_397554), 6xHis tag (ab18184, Abcam, RRID:AB_444306), anti DMC1 (ab11054, Abcam, RRID:AB_297706), anti SYCP3 (AF3750, R&D systems, RRID:AB_2197194), anti SYCP1 (Meuwissen et al.,

1992), anti HORMAD1 (Wojtasz et al., 2009). Anti-HSF2BP rabbit polyclonal antibodies SY8126 and SY8127 were raised against purified recombinant untagged human HSF2BP (Kaneka Eurogentec, Belgium) and used either as crude serum or after affinity purification against GST-HSF2BP immobilized on glutathione Sepharose as described (Chalkley and Verrijzer, 2004). The BRCA2 antibody was raised against residues 1842–2080 of xIBRCA2. The cDNA encoding the fragment was codon-optimized for *E. coli*, synthesized (gBlocks Gene Fragments, Integrated DNA Technologies), and ligated into the Xhol-BamHI sites of the pETDuet-1 vector (Novagen). The fragment was overexpressed in *E. coli* BL21(DE3) cells (New England BioLabs) with a N-terminal His-tag, and purified by the method described previously (Klein Douwel et al., 2014). The purified antigen was used for immunization of rabbits (PRF&L, Canadensis, USA). Specificity of the antisera was confirmed using immunoblotting.

To prepare total protein lysates, cells were scraped in PBS and lysed in 2x Laemmli SDS loading buffer (120 mM Tris pH 6.8, 4% SDS, 10% Glycerol), after determining the protein concentration in the lysate by Lowry method, the lysate was complemented by 10x reducing additive (0.1% bromophenol blue, 0.5% β-mercaptoethanol). Mouse tissues were homogenized using Tissuelyzer (QIAGEN) in 2x Laemmli buffer. Proteins were separated on polyacrylamide handcast tris-glycine, or precast bis-tris or tris-acetate gels (Novex) and blotted on nitrocellulose or PVDF. For BRCA2 detection 4%–8% precast tris-acetate gels were used, and transfer was performed in 2x Towbin transfer buffer (50 mM Tris, 384 mM glycine, 20% methanol) at 300 mA constant current for 2h at 4°C to PVDF membrane. Membranes were blocked in 3% milk in PBS+0.05% Tween. After overnight incubation with the primary antibody, membranes were washed in PBS+0.05% Tween and incubated with horseradish peroxidase-conjugated secondary antibodies (Jackson Immunoreserach). Blots were developed using homemade ECL reagents and detected with the Alliance 4.7 (UVPtec).

Protein Purification

Human HSF2BP cDNA was re-cloned into pETM11 (6xHis-TEV) expression vector using Gibson assembly and transformed into *E. coli* Rosetta2 (DE3) pLysS. A starter culture (LB + 50 µg/ml kanamycin, 30 µg/ml chloramphenicol) was grown overnight at 37°C, used to inoculate 4.5 L of LB which was grown at 37°C until the OD₆₀₀ reached 0.6. Expression was induced by addition of IPTG to 0.2 mM, incubation was continued at 16°C for 16 h, cells were harvested and frozen, thawed in equal volume of 2x lysis buffer (1M NaCl, 25mM Tris pH7.5, 5% Glycerol, 5 mM β-mercaptoethanol, 1x EDTA-free protein inhibitor cocktail (Roche)) and sonicated (8x 30 s). The lysate was cleared by centrifugation at 35,000 rcf. for 45 min, and loaded on Ni-NTA beads equilibrated with binding buffer (500 mM NaCl, 25mM Tris pH7.5, 5% Glycerol, 5 mM β-mercaptoethanol). Beads were washed with increasing concentration of imidazole (20 and 40 mM) in binding buffer. Fractions were eluted with 250 mM imidazole and analyzed by SDS-PAGE. Fractions containing HSF2BP were pooled and loaded on Superdex 200 16/60 gel filtration column equilibrated with GF buffer(250 mM NaCl, 25 mM Tris pH7.5, 5% Glycerol, 5 mM β-mercaptoethanol) on an ÄKTA FPLC system (GE Healthcare). Peak fractions containing HSF2BP were pooled and further purified on a 5 mL HiTrap Q anion exchange column using a gradient from 100 till 600 mM NaCl in 25 mM Tris pH7.5, 5% Glycerol, 5 mM β-mercaptoethanol. Fractions containing HSF2BP were pooled, concentrated, flash-frozen in GF buffer using liquid nitrogen and stored at –80°C. To produce HSF2BP without his-tag, HSF2BP eluted from the Ni-NTA beads was mixed with Tobacco Etch Virus (TEV) protease and dialyzed o/n at 4°C against GF buffer before loading onto the gel filtration column. HSF2BP variant R200T was purified as wild-type. HSF2BP concentration was determined spectrophotometrically ($\epsilon^{280\text{nm}} = 20970 \text{ M}^{-1} \text{ cm}^{-1}$).

Human BRCA2 fragment F6 (Gly2270–Asp2479) was cloned into pETM-30 (6xHis-GST-TEV) expression vector and purified and stored according to the protocol described above for HSF2BP, without removal of the tag. Concentration of the fusion protein was determined spectrophotometrically using $\epsilon^{280\text{nm}} = 52830 \text{ M}^{-1} \text{ cm}^{-1}$. BRCA2 fragment F8 (Gly2270–Ala2351) was cloned into pETM11 and purified and stored according to a protocol similar to that for HSF2BP, up to and including TEV cleavage to remove the tag. Subsequently the dialyzed material was loaded onto a 5 mL HiTrap S cation exchange column. BRCA F8 eluted in the flow through, was concentrated and further purified on a Superdex 75 16/60 size exclusion chromatography column (GE Healthcare) equilibrated with GF buffer. Concentrated fractions were flash frozen and stored at –80°C. The F8 concentration was estimated using SDS-PAGE with Coomassie Brilliant Blue staining, using bovine serum albumin (BSA) as the standard.

The cDNA encoding full-length xHSF2BP was codon-optimized for *E. coli*, synthesized (gBlocks Gene Fragments, Integrated DNA Technologies), and ligated into Xhol-BamHI sites of the pETDuet-1 vector. xHSF2BP was overexpressed with a N-terminal His-tag in *E. coli* BL21(DE3) cells at 18°C. The cells were collected by centrifugation, resuspended in buffer A (50 mM Tris pH 8.0, 10% glycerol, 500 mM NaCl, 1 mM phenylmethylsulphonyl fluoride, 10 mM imidazole, and 5 mM DTT), and disrupted by sonication. The soluble fraction was collected by centrifugation at ~40,000 × g for 25 min at 4°C, and mixed gently with 1 mL Ni-NTA agarose resin (Life Technologies) at 4°C for 1 h. The Ni-NTA agarose resin was packed into Poly-Prep chromatography column (Bio-Rad), and washed with 50 mL buffer A containing 20 mM imidazole. The xHSF2BP protein was eluted with 8 mL buffer A containing 400 mM imidazole, and concentrated using a 30 kDa MWCO Amicon Ultra-15 centrifugal filter unit (Millipore). The sample was then loaded onto a Superdex 200 column (HiLoad 16/60 preparation grade, GE Healthcare) equilibrated with buffer B (25 mM Tris pH 7.5, 5% glycerol, 200 mM NaCl, and 5 mM DTT). The eluted xHSF2BP protein was concentrated, and aliquots were flash frozen with liquid nitrogen. The protein concentration was determined by SDS-PAGE with Coomassie Brilliant Blue staining, using bovine serum albumin (BSA) as the standard protein.

Sequence and expression analysis

HSF2BP domain composition analysis and structure prediction were performed using Phyre2 server (Kelley et al., 2015). The armadillo repeat region is predicted starting at residues 100–140 with high confidence (e.g., 97% confidence for the model for A109-V334 of hHSF2BP by Phyre2 based on β-catenin structure PDB: 3SLA, which has 19% sequence identity). Public RNA-seq data was analyzed using GEPIA server (Tang et al., 2017). Expression levels in mES were taken from two RNA-seq datasets (Lienert et al., 2011; Wamstad et al., 2012), each with two biological replicates. Search for homologs was performed using hmmsearch software (Potter et al., 2018).

Analytical Gel Filtration

A Superdex 200 increase 3.2/300 (GE Lifesciences) was equilibrated with GF buffer on an ÄKTA Micro system (GE Healthcare). In a total volume of 50 µl, 37 µM untagged HSF2BP (wild-type or R200T) and/or 60 µM BRCA2-F8, was applied to the column at a flow of 50 µl/min. 50 µl fractions were collected and analyzed using SDS-PAGE (15% acrylamide).

GST Pull-down

20 µl of glutathione beads were prewashed with buffer (150 mM NaCl, 25 mM Tris pH 7.5, 5% Glycerol, 5 mM β-mercaptoethanol). 200 µmol of GST or GST-BRCA2 F6 was bound for 1 h at 4°C. Beads were washed 3x with buffer. 500 µmol of HSF2BP (WT or R200T) was added and incubated for 1 hr at 4°C. Beads were washed 3x with buffer. Samples were analyzed on SDS-PAGE.

Immunoprecipitation (IP)

For co-IP mES cells were washed twice in ice-cold PBS and lysed *in situ* in NETT buffer (100 mM NaCl, 50 mM Tris pH 7.5, 5 mM EDTA pH 8.0, 0.5% Triton X-100) supplemented immediately before use with protease inhibitor cocktail (Roche) and 0.4 mg/ml Pe-fabloc (Roche) (NETT++). Four hundred fifty µl NETT++ buffer was used per 145 mm dish. After 30 min lysis on ice, mixtures were centrifuged (15 min, 4°, 14000 rcf.) and the supernatant (input) was added to washed anti-GFP beads (Chromotek). Beads and lysates were incubated 2–4 h at 4°C while rotating, washed three times in NETT++ buffer and bound proteins were eluted by boiling in 2x Sample buffer.

IP from *Xenopus* egg extracts was performed as described previously with modifications (Knipscheer et al., 2009). 3 µl BRCA2 or HSF2BP antiserum was incubated with 30 µl Protein A Sepharose Fast Flow (PAS) beads (GE Healthcare) overnight at 4°C. The beads were washed twice with 400 µl PBS, once with 400 µl ELB (10 mM HEPES-KOH (pH 7.7), 50 mM KCl, 2.5 mM MgCl₂, and 250 mM sucrose), twice with 400 µl ELB supplemented with 0.5 M NaCl, and finally twice with 400 µl ELB supplemented with 0.25 mg/ml BSA. For IP with BRCA2 antiserum, 5 µl of the antibody-bound beads were incubated with 20 µl diluted NPE (4 µl NPE and 16 µl ELB) for 1 h at 4°C. 1.5 µl HSF2BP (3 µM) was then added to the beads, and the reaction mixture was incubated for 3 h at 4°C. The beads were washed 4 times with 400 µl ELB containing 80 mM NaCl and 0.5% Triton X-100 (Sigma). For IP with HSF2BP antiserum, 5 µl of the antibody-bound beads were incubated with 2 µl HSF2BP (3 µM) for 1 h at 4°C, and washed twice with 400 µl ELB supplemented with 0.25 mg/ml BSA. The beads were then incubated with 20 µl diluted NPE (4 µl NPE and 16 µl ELB) for 3 h at 4°C, and washed 4 times with 400 µl ELB. The bound proteins were eluted by adding 10 µl 1x SDS sample buffer (75 mM Tris pH 6.8, 10% glycerol, 2.5% SDS, 50 mM TCEP (Bond-Breaker TCEP solution, Life Technologies), and 0.025% Bromophenol blue), separated by SDS-PAGE, and detected by western blotting with RAD51 (1:10,000), BRCA2 (1:1,000), or HSF2BP (1:2,500) antiserum. Preimmune serum was used for mock immunoprecipitation.

Immunofluorescence and Microscopy

Direct HSF2BP-GFP imaging and immunofluorescence staining was performed on ES cells grown overnight on a glass coverslip coated with laminin, which improves their attachment and morphology. Sterile 24 mm coverslip was placed in a 6-well plate, and a 100 µl drop of 0.05 mg/ml solution of laminin (Roche, 11243217001) was pipetted in the middle of it. The plate was left for ~30 min in the cell culture incubator, after which the laminin solution was aspirated, and cell suspension was placed in the well. DNA damage was induced by irradiation with 8 Gy X-ray followed by 2 h recovery, treatment with 1 µg/ml Mitomycin C (MMC, Sigma, M4287) for 2 h followed by 2 h recovery, or incubation with 0.1 µM talazoparib (BMN 673, Axon Medchem, #2502) overnight. Cells were washed with PBS, fixed for 15 min in 2% paraformaldehyde in PBS at room temperature and mounted in VectaShield with DAPI either directly, or after immunostaining with anti-53BP1 (Novus Biologicals, NB100-304, RRID:AB_10003037, 1:1000) or anti-geminin (Proteintech, 10802-I-AP, RRID:AB_2110945, 1:400) antibody. Images were acquired using Leica SP5 confocal microscope. Maximum projections from a z stack of 3–5 confocal planes through a 1 µm slice were produced for analysis.

Oblique illumination microscopy and particle tracking were performed exactly as described (Reuter et al., 2014) using inverted Nikon Eclipse Ti-E microscope equipped with a Plan Apo TIRF objective (100x, N.A. 1.49, oil) and a QuantEM EMCCD camera (Roper Scientific); a 491 nm Calipso diode-pumped solid-state laser (Cobolt) at 5–7 mW power at the objective back-focal-plane; built-in Nikon Ti TIRF-E motorized illumination unit; Chroma ET-GFP filter cube with an HQ530/30M emission filter; the excitation filter was removed; the hardware was controlled with MetaMorph 7.5 software (Molecular Devices). Video streams containing typically 200 frames (16-bit) were collected continuously using the full camera chip without binning, a frame acquisition time of 50 ms and an EM Gain of 950 (3x). The lookup table was linear and covered the full range of the data. Live-cell imaging was carried out in cell growth medium under a 5% CO₂ atmosphere and at 37°C using a Tokai Hit stage heating system; coverslips were not coated

with laminin. The experiment was repeated three times, two independent *Hsf2bp*^{GFP/+} clones were used in each. Duration of mobile and immobile states under control conditions (Figure 1G, left column) or 2 h after irradiation with 10 Gy (middle), and the difference between the two (right) were plotted. Image analysis was performed using the ImageJ (ImageJ, RRID: SCR_003070) plugin and MATLAB scripts described in (Reuter et al., 2014).

Fresh testes from wild-type and *Hsf2bp*^{-/-} male mice were processed to make meiotic nuclear spread preparations as described previously (Peters et al., 1997). Triple staining of RAD51 (1:1000), DMC1 (1:1000) and SYCP3 (1:75) and double staining of SYCP1 (1:5000) and HORMAD1 (1:100) was performed as described (Carofiglio et al., 2013). Confocal images were taken using a Zeiss LSM700 confocal, equipped with a digital camera.

Hsf2bp knockout mouse model

Female donor mice (age 5 weeks, C57BL/6 OlaHsd from Envigo) were superovulated by injecting 5-7.5 IE folligonan (100-150 µl, IP (FSH hormone; time of injection ± 13.30 h; day -3). Followed at day -1 by an injection of 5-7.5 IE chorulon (100-150 µl, IP (hCG hormone; time of injection 12.00 h). Immediately after the chorulon injection, the females were put with fertile males in a one to one ratio. Next day (0) females were euthanized by cervical dislocation. Oviducts were isolated, oocytes collected and injected with ribonucleoprotein complexes of S.p.Cas9 3NLS (IDT cat. no. 1074181), crRNA and tracrRNA (both Alt-R, synthesized by IDT). Target sequences for crRNA were ACTGCAGTAGTAAACGGAGG (upstream of *Hsf2bp* exon 3) and ACTGCTGGATCAACTGTTTA (downstream of exon 6). For ribonucleoprotein formation equal volumes (5 µL) of crRNA and tracrRNA (both 100 µM in IDT annealing buffer) were mixed, heated to 95°C for 5 min and allowed to cool on the bench. The annealed RNAs (1.2 µL, 50 µM) were mixed with Cas9 (10 µl diluted to 200 ng/µl in the DNA microinjection buffer (10 mM Tris-HCl, pH 7.4, 0.25 mM EDTA in water) at the final concentrations 0.12 µM Cas9, 0.6 µM of each of the two crRNA:tracrRNA complexes in microinjection buffer. Foster mothers (minimum age 8 weeks) were set up with vasectomized males in a 2 to 1 ratio. Next day (0), pseudopregnant females (recognized by a copulation prop) were collected. For transplanting the injected oocytes, pseudopregnant females were anesthetized by an IP injection of a mix of Ketalin (12 mg/ml ketamine in PBS)-Rompun (0.61 xylazine mg/ml PBS) 100 µL per 10 g bodyweight). Post-surgery pain relief was given when the mouse was anaesthetized (S.C. Rimadyl Cattle, 5mg/ml in PBS, dose 5 µg/g mouse). Transplantation resulted in 21 pups from three litters, of which 8 (7 males, 1 female) contained the expected deletion allele as determined by PCR genotyping with primers mHSF2BP-geno-F1 actacccctactgttagcat, mHSF2BP-geno-F2 gccagctgctctcttagt, mHSF2BP-geno-F3 tggctgtgaattcttgtga, mHSF2BP-geno-R1 tcatctggggccactagtaa and mHSF2BP-geno-R2 atgcataaccgcgcacacaa used in different combinations. The founder animals were backcrossed and intercrossed to produce the experimental cohort. Routine PCR genotyping was performed using MyTaq Red mix (Bioline) and a combination of three genotyping primers: mHSF2BP-geno-F2, mHSF2BP-geno-F3 and mHSF2BP-geno-R1, which allows simultaneous amplification of the wild-type and the deletion alleles (PCR products 434 and 586 bp, respectively).

Adult wild-type and *Hsf2bp*^{-/-} males were sacrificed and weighed, and testes and epididymides were collected and also weighed. Epididymides were collected in PBS, dounced, and sperm cells were counted. From each animal 1 testis was fixed in Bouin solution overnight and further processed for histological analysis using standard methods. The other testis was placed in PBS and further processed for immunocytochemistry as described in the corresponding section. For fertility assessment breedings were set up between *Hsf2bp*^{-/-} and wild-type C57BL/6 animals and maintained for 6 weeks.

QUANTIFICATION AND STATISTICAL ANALYSIS

Statistical details of experiments can be found in figure legends or in the text of the [Results](#) section if data is not plotted, n represents the number of independent experiments or number of animals analyzed. Quantitative functional experiments on knockout cells were repeated at least three times, with at least two independent clones per mutant genotype; data from independent clones was treated as biological replicates and are plotted separately. In clonogenic survival plots mean values and s.e.m are plotted. For other plots individual values are shown, lines indicate means and s.d. Measurements from all analyzed animals are plotted, no data was excluded. Statistical analysis and curve fitting were performed using GraphPad Prism software. Statistical significance was determined using Student's t test, or χ^2 test for genotype frequencies. Significance levels are indicated on the plots as * p < 0.05, ** p < 0.001, *** p < 0.0001, **** p < 0.0001.